Heat Transfer Enhancement by Electromagnetic Forcing in Duct Flow

Rawad Himo, Charbel Habchi

Heat Transfer Enhancement by Electromagnetic Forcing in Duct Flow

Rawad HIMO[1,2*], **Charbel HABCHI**[2]

[1]University of Nantes, Laboratoire de Thermique et Energie de Nantes (LTeN) UMR CNRS6607, B.P. 50609, 1 rue Christian Pauc, 44306 Nantes Cedex 3, France
[2] Notre Dame University - Louaize, Thermofluids Research Group, Zouk Mosbeh, Lebanon
*(Corresponding author: rawad.himo@univ-nantes.fr)

Abstract - Electromagnetic forcing could be used to produce streamwise vortices in order to enhance the heat and mass transfer processes in ducts and pipes. In our current study we take this novel method to a more practical use, to suggest a Magneto hydrodynamic heat exchanger in which several transverse Lorentz forces are arranged along the streamwise direction to produce secondary flow structures and enhance mixing of hot fluid particles near the wall with cold fluid particles near the center. The Reynolds number based on the mean flow velocity and hydraulic diameter is taken 1000. The flow structures, the local heat transfer and the thermal performances are quantitatively analyzed to show the effectiveness of this concept. Increases by more than 100% in the global Nusselt number and the thermal performance were detected. Several configurations of forcings were tested, where it was found that the increase in local and global Nusselt is more efficient with subsequent forces of the same direction, rather than changing directions.

Nomenclature

A	overall area of heat transfer, m^2	S	exchange area, m^2
$\mathbf{B}$	magnetic field, T	T	temperature, K
c	heat capacity of the fluid, $\mathrm{J/kgK}$	ΔT_{lm}	log mean temperature difference, K
$\mathbf{F}$	Lorentz force, $\mathrm{N/m}^3$	$\mathbf{u}$	velocity vector field, $\mathrm{m/s}$
GCI	Grid convergence index		
h	convective heat transfer coefficient, $\mathrm{W/m^2K}$	*Greek symbols*	
$\mathbf{J}$	current density, $\mathrm{A/m}^3$	ρ	density, $\mathrm{kg/m}^3$
k	bulk fluid thermal conductivity, $\mathrm{W/mK}$	μ	dynamic viscosity, $\mathrm{Pa.s}$
Nu	global Nusselt number	ϕ	electric field scalar potential, V
Nu_z	local Nusselt number	σ	electric conductivity of the fluid, S
p_c	apparent order of converge		
q	overall rate of heat transfer, W		

1. Introduction

Vortex Generators have been extensively studied and used in multifunctional heat exchangers/reactors to enhance heat and mass transfer. While, two main types of vortices can be distinguished, namely: longitudinal and transverse. Previous studies [1] proved that longitudinal VGs, having a principal axis in the direction of the flow, are more efficient since they induce swirling motions, not otherwise witnessed in the quasi-2D flows generated by transverse VGs.

Different shapes and angles of attack for the inserts have been addressed in the literature to generate longitudinal as well as transverse vortices [2, 3, 4]; hence, the two aforementioned control parameters (shape and angle of attack) affect the flow structure, in addition to the evident

importance of the main flow's Reynolds number. Extensive attempts of studying the shapes and orientations of vortex generators remain mostly stochastic design problems that are relatively time consuming, experimentally and numerically. In the present work, we intend to generate vortices in the flows by using electromagnetic forcing to mimic vortex generators, this type of flows is also known as magneto-hydrodynamics (MHD). Consequently, we transform our control parameters from the geometric features of the vortex generators to the magnitude of the electrical potential and magnetic field; which in fact are more easily controlled by simply adjusting the intensities of the two entities [5].

Many studies in the open literature were performed to analyze the convective heat transfer enhancement in MHD flows [6, 7, 8, 9]. Motozawa *et al.* [10] studied experimentally the convective heat transfer in rectangular smooth duct flow of a magnetic fluid at a Reynolds number of 780. As expected, the local Nusselt increased in the proximity of the external magnetic field. A maximum recorded increase of the Nusselt number was 20%. Considering the difficulty of visualizing the flow, the study did not include an analysis of the flow structure vis-à-vis the heat transfer enhancement. More specifically, an experimental study on MHD flows using a potassium hydroxide solution (KOH) revealed that for low Reynolds numbers the MHD effects are more prominent due to weaker production of turbulence [11]. It is also important to mention that numerical studies have shown that the pressure drop for electrically insulated ducts is lower than electrically conducting walls due to eddy currents generated near the electrically conducting walls [12].

Our previous work showed that by using a transverse Lorentz force in a duct flow where the working fluid is an aqueous solution of 25% wt. KOH; heat transfer is enhanced locally and globally due to the coherent structures that were generated and were correlated to the increase in heat transfer [5]. In this current study, we upgrade this novel method of heat transfer to cater for industrial applications, whereby we use a higher Reynolds number and different configurations of subsequent Lorentz forces to further increase the overall heat transfer.

The paper is organized as follows: the computational domain and numerical procedure are presented in section 2, then the results are discussed in section 3. Finally, section 4. is devoted for the concluding remarks.

2. Problem description

2.1. Governing equations

The flow field is governed by the three-dimensional (3D) steady Navier Stokes equations. The continuity and momentum equations for an incompressible Newtonian fluid in presence of electromagnetic forcing are as follows:

$$\nabla \cdot \mathbf{u} = 0 \tag{1}$$

$$\mathbf{u} \cdot \nabla \mathbf{u} = -\frac{1}{\rho}\nabla p + \frac{1}{\rho}\nabla \cdot \left[\mu \left(\nabla \mathbf{u} + \nabla \mathbf{u}^T\right)\right] + \frac{\mathbf{F}}{\rho} \tag{2}$$

where $\mathbf{F} = \mathbf{J} \times \mathbf{B}$ is the Lorentz force, with $\mathbf{J}$ the current density and $\mathbf{B}$ the external magnetic field.

In the present study, the boundary conditions are for fixed electric potential. Thus Ohm's law

is used here to determine the current density as follows:

$$\mathbf{J} = \sigma \left[-\nabla\phi + (\mathbf{u} \times \mathbf{B}) \right] \tag{3}$$

where ϕ is the electric field scalar potential and σ the electric conductivity of the fluid.

The conservation of electric charge enforces:

$$\nabla \cdot \mathbf{J} = 0 \tag{4}$$

Therefore Eq. (3) reduces to

$$\nabla^2\phi = \nabla \cdot (\mathbf{u} \times \mathbf{B}) \tag{5}$$

The energy equation for forced convection is also computed in the fluid domain and is given by:

$$\rho c_p \nabla \cdot (\mathbf{u}T) = k\nabla^2 T + \frac{1}{\sigma}\mathbf{J}.\mathbf{J} \tag{6}$$

where c_p is the specific heat and k is the bulk molecular thermal conductivity.

In the present study, the buoyancy effects are negligible compared to the inertial and viscous ones. Consequently, the convection remains forced as per the flow's Reynolds and Rayleigh numbers [14].

2.2. Numerical procedure

The solver used for the flow computation is the CFD code ANSYS Fluent 18.0 [15], which is based on cell-centered finite volume discretization method. The governing equations are solved sequentially with double precision and a second-order upwind scheme [16] for spatial discretization of the convective terms. The diffusion terms are central differenced and second-order accurate. Pressure-velocity coupling is achieved by the Coupled algorithm [15].

The walls are electrically insulated except for the conducting electrodes. The working fluid is an aqueous solution of 25% potassium hydroxide KOH, with dynamic viscosity varying with the fluid temperature [17] according to a polynomial function given in Eq. (7):

$$\mu = 4.917 \times 10^{-7} T^2 - 3.348 \times 10^{-4} T + 5.793 \times 10^{-2} \tag{7}$$

Flow and heat-transfer simulations are carried out for a Reynolds number of 1000, based on the mean flow velocity and the hydraulic diameter, and for uniform wall temperature $T_w = 350$ K. For Reynolds numbers above 1000, higher electrical potential is required to affect, making it less practical for industrial applications. The temperature of the inlet of the computational domain is uniform $T_{in} = 300$ K. Atmospheric pressure is prescribed at the domain outlet. No-slip boundary conditions are prescribed on all solid surfaces. The residual value 10^{-6} is set as the convergence criterion for the solutions of the flow and energy equations. Beyond this value no significant changes were observed in the velocity and temperature fields. It is equally important to note that this numerical method has been validated with DNS results in our previous study [5].

2.3. Computational domain and meshing

The computational domain consists of a square duct of hydraulic diameter $D_h = 10\text{mm}$, with four pairs of electrodes starting from the position $z = 2.5 \times D_h$ and spaced by a distance of $5 \times D_h$. The electrode width (in the flow direction) is equal to $D_h/2$. The electrodes are embedded inside the duct material, therefore the computational domain has a constant cross sectional area. A uniform magnetic field $|\mathbf{B_{0,y}}| = 50\ \text{mT}$ is applied in the streamwise direction starting at location where the electrodes are turned on. Therefore an electromagnetic force will be generated at such locations.

The arrangement and polarity of electrodes is chosen in order to obtain forces in the transverse direction to generate secondary flows and mimic the common flow up induced by the pressure gradients across vortex generators which are used for heat and mass transfer enhancement [18, 4]. Five different configurations of electrodes are considered in this study and are all compared with the empty duct flow. The different configurations are summarized in Table 1. In this table configuration (6) corresponds to the empty duct flow without forcing. Configuration (1) is shown in Figure 2 (a).

Electrode Row	1^{st}	2^{nd}	3^{rd}	4^{th}
Streamwise Location	$\frac{5D_h}{2}$	$\frac{16D_h}{2}$	$\frac{27D_h}{2}$	$\frac{38D_h}{2}$
Configuration (1)	Flow up	Flow left	Flow down	Flow right
Configuration (2)	Flow up	Flow up	Flow up	Flow up
Configuration (3)	Flow up	off	Flow left	off
Configuration (4)	Flow up	off	Flow up	off
Configuration (5)	Flow up	off	off	off
Configuration (6)	off	off	off	off

Table 1 : *Flow configurations*

Non-uniform structured three-dimensional meshes were generated while paying special attention to the near-wall refinement at all solid boundaries (duct wall and electrodes) so as to take into account the high velocity and temperature gradients in these regions. The different mesh densities and their main features are given in Table 2.

To determine the appropriate mesh density for solution grid independence, the solver is run with increasing mesh densities until no significant effect on the results is detected. The mesh validity verification is performed by using the method proposed by Celik [19] where the grid convergence index (GCI) and the apparent order of convergence p_c can be obtained. The mesh validity verification is applied to the global Nusselt number Nu obtained from Eq.8, representing the ratio of convective to conductive transfer:

$$Nu = \frac{hD_h}{k} \tag{8}$$

where h is the overall convective heat transfer coefficient $(\text{W/m}^2\text{K})$, D_h the hydraulic diameter, and k is the bulk thermal conductivity of the working fluid.

In Eq.8 h is calculated from the logarithmic mean temperature difference:

$$h = \frac{\dot{q}}{A\Delta T_{lm}} \tag{9}$$

Cell number n	$638,880$	$1,103,937$	$1,827,011$
Mesh size $l = (V/n)^{1/3}\,(\mathrm{mm})$	0.0536	0.0446	0.0378
Global time-averaged Nusselt number $\overline{Nu}$	12.291	12.274	12.266
Grid Convergence Index $GCI(\%)$	–	–	0.17
Apparent order of convergence p_c	–	–	1.77

Table 2 : *Mesh sensitivity analysis*

where $\dot{q}$ is the overall rate of heat transfer (W) defined in Eq.10, $A(\mathrm{m}^2)$ is the heat transfer area and ΔT_{lm} is the logarithmic mean temperature difference defined in Eq.11.

$$\dot{q} = \dot{m} c_p \Delta T \tag{10}$$

where $\dot{m}$ is the mass flow rate (kg/s) and $\Delta T = T_{out} - T_{in}$ is the bulk temperature difference between the inlet and outlet:

$$\Delta T_{lm} = \frac{(T_w - T_{in}) - (T_w - T_{out})}{ln(\frac{T_w - T_{in}}{T_w - T_{out}})} \tag{11}$$

As shown in Table 2, the uncertainty in the fine-grid solution is found to be about 0.17% and the order of convergence is 1.77. For more details about the calculation of the parameter GCI and p_c, the readers can refer to Celik [19]. It should be noted that the mesh study presented here is performed for configuration (1) which induces high gradients considering the changing direction of the Lorentz forces.

The numerical simulations are performed on eight parallel Intel® Core™ i7-7700 2.80 GHz processors. Each run takes between 12 and 36 hours.

3. Results and discussion

3.1. Temperature distribution

The temperature distribution of the six tested configurations is shown in Figure 1 at four different cross section. It can be clear from configurations (1) and (3), where the forcing changes directions, that the flow structure and temperature distributions change with the changing direction of the imposed Lorentz forces. On the other hand, for configurations (2) and (4) the direction doesn't change. As a result, the flow structure and temperature distributions, highlighted by the primary vortex counter-rotating pair, is further energized after each force instead of being destroyed, leading to more growing secondary vortices near the corners and side walls. Consequently, the secondary flows enhance the advective heat transfer from the hot walls to the cold fluid.

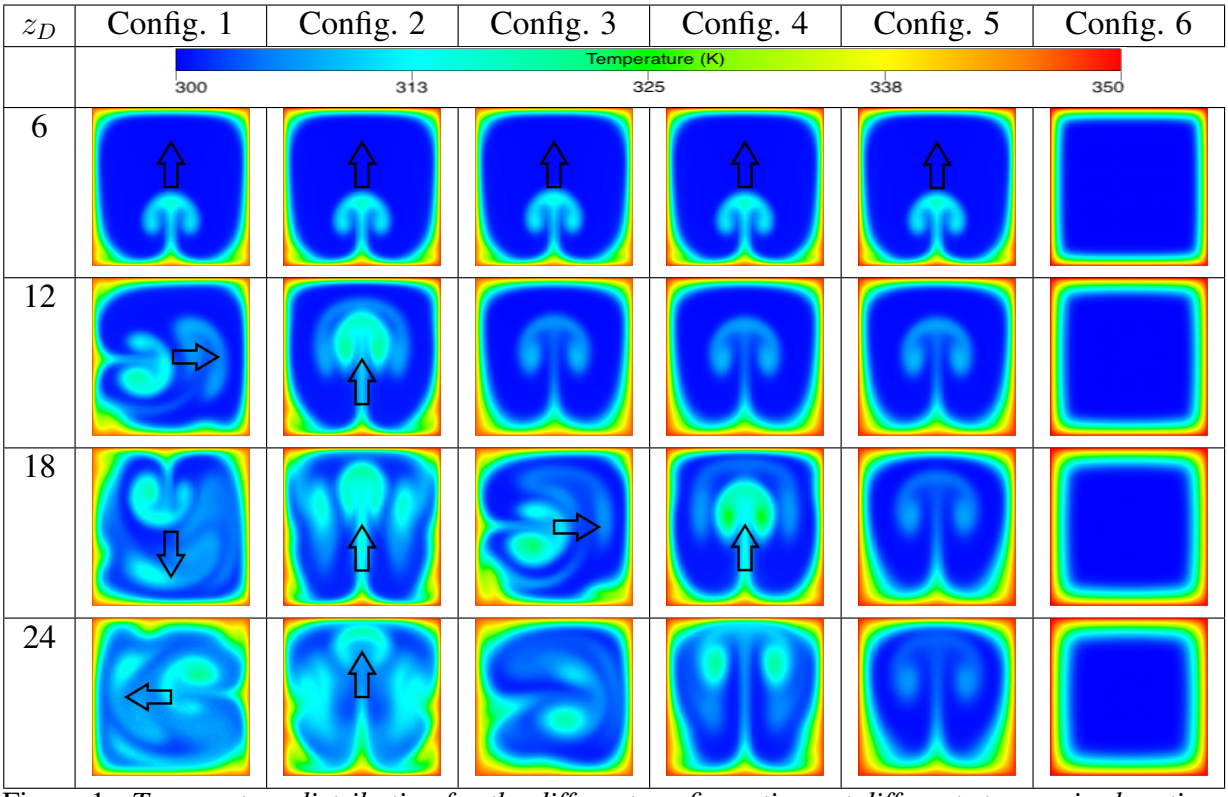

Figure 1 : *Temperature distribution for the different configurations at different streamwise locations* $z_D = z/D_h$

3.2. Local and global results

The local Nusselt numbers of each configuration is shown in Figure 2 (a) where the effect of the forces on the heat transfer manifest clearly with local increases that begin at the location of the applied force and carry on along the streamwise direction. It is obtained from the span-averaged heat flux at every streamwise position. From Figure 2 (a) the two configurations (1) and (2) can be compared, in addition to also (3) and (4). It is obvious that configuration (2) provide better heat exchange than (1), as is the case for configuration (4) compared to (3); despite having the same input electromagnetic force, where only the direction is varied.

One can therefore summarize those results in a plot showing the global Nusselt number vs the number of forces for both same and different directions of the forces. The global Nusselt is calculated from the log mean temperature method explained in section 2.3. As vorticity is induced more heat is exchanged from to hot walls to the cold fluid, this will in turn raise the average temperature at the end of the duct. This plot in Figure 3 (a) confirms our conclusion from the local results, that having consecutive forces of the same direction is more efficient than changing directions. The thermal performance enhancement introduced in Equation 12 based on the same pumping power [5] is shown in Figure 3 (b) where it can be deduced that despite the increase in friction, thermal performance is improved up to 102% for the same direction forcings and up to 89% for the changing direction. Lastly, it is worthy to note that the difference between the changing and non-changing configurations increases as the number of forces increase and therefore this study leads to the recommendation of using non-changing transverse Lorentz forces for higher efficiency in industrial applications.

$$\eta = \frac{Nu}{Nu_0} \cdot \left(\frac{f}{f_0}\right)^{-\frac{1}{3}} \tag{12}$$

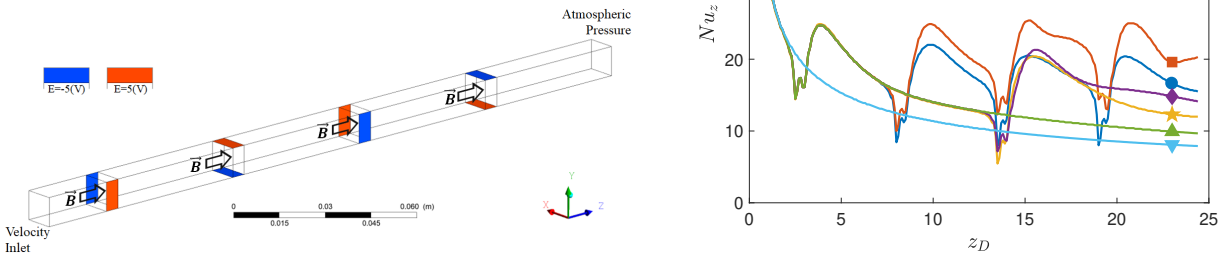

(a) (b)

Figure 2 : *Setup for Configuration 1, with positive (in red) and negative (in blue) electrodes (a), and local Nusselt number for the different configurations (b)*

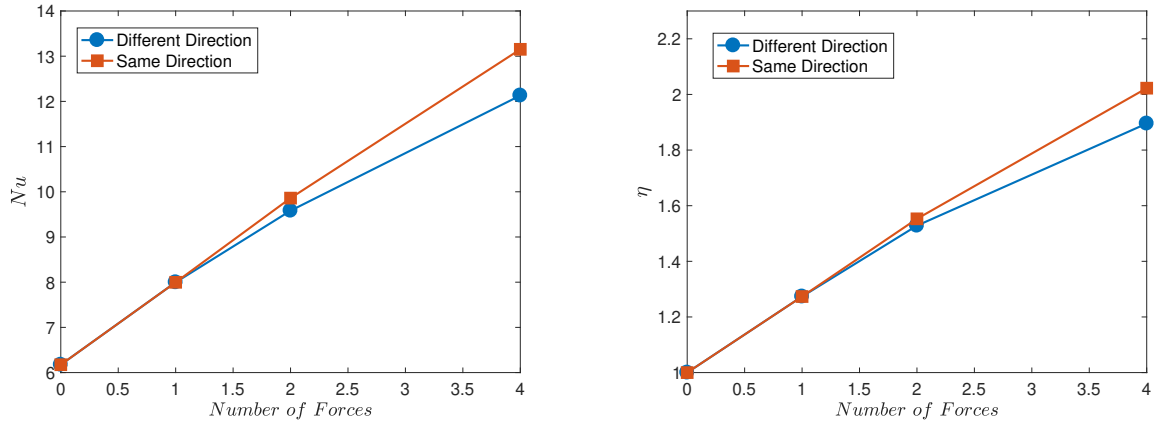

(a) (b)

Figure 3 : *Global Nusselt (a) and thermal performance enhancement coefficient (b) for the different configurations vs the number of forces*

4. Conclusion

The effect of electromagnetic forces in conducting fluid duct flow on the heat transfer has been studied and the results can be summarized below:

• Transverse Lorentz forces in conducting fluid flows improves convective heat transfer by inducing vorticity.

• The global Nusselt number can be increased by more than 100% when using Lorentz forces as vortex generators

• When using consecutive forces, having the same direction is more efficient than changing directions of the forces.

References

[1] M. Fiebig, Vortices, Generators and Heat Transfer, *Chemical Engineering Research and Design*, 76 (1998) 108-123.

[2] T.V. Buren, E. Whalen, M. Amitay, Interaction between a vortex generator and a synthetic jet in a crossflow, *Physics of Fluids*, 27 (2015) 107101.

[3] M. Oneissi, C. Habchi, S. Russeil, D. Bougeard, T. Lemenand, Novel design of delta winglet pair vortex generator for heat transfer enhancement, *International Journal of Thermal Sciences*, 109 (2016) 1-9.

[4] A. M. Hamed, A. Pagan-Vazquez, D. Khovalyg, Z. Zhang, L.P. Chamorro, Vortical structures in the near wake of tabs with various geometries, *Jounral of Fluid Mechanics*, 825 (2017) 167-188.

[5] R. Himo, C. Habchi, Coherent flow structures and heat transfer in a duct with electromagnetic forcing, *Physics of Fluids*, 30 (2018) 043605.

[6] H. Huang, B. Li, Heat transfer enhancement of free surface MHD-flow by a protrusion wall, *Fusion Engineering and Design*, 85 (2010) 1496-1502.

[7] I.A. Melnikov, E.V. Sviridov, V.G. Sviridov, N.G. Razuvanov, Experimental investigation of MHD heat transfer in a vertical round tube affected by transverse magnetic field, *Fusion Engineering and Design*, 112 (2016) 505-512.

[8] O. G. Cassells, W. K. Hussam, G. J. Sheard, Heat transfer enhancement using rectangular vortex promoters in confined quasi-two dimensional magnetohydrodynamic flow, *International Journal of Heat and Mass Transfer*, 93 (2016) 186-189.

[9] T. Alam, M.H. Kim, A comprehensive review on single phase heat transfer enhancement techniques in heat exchanger applications, *Renewable and Sustainable Energy Reviews*, 81 (2018) 813-839.

[10] M. Motozawa, J. Chang, T. Sawada, Y. Kawaguchi, Effect of magnetic field on heat transfer in rectangular duct flow of a magnetic fluid, *Proc. Physics Procedia 12th International Conference on Magnetic Fluids (ICMF12)* (2010), 190–193.

[11] T. Junichi, Experimental investigation of magnetohydrodynamic turbulent pipe flow of aqueous electrolyte solution, *PhD Thesis University of California LA* (2009).

[12] P. J. Bhuyan, K. S. Goswami, Effect of magnetic field on MHD pressure drop inside a rectangular conducting duct, *IEEE Transactions on Plasma Science*, 36 (2008) 1955-1959.

[13] F.R. Menter, Two-Equation Eddy-Viscosity Turbulence Models for Engineering Applications, *AIAA Journal*, 32 (1994) 1598-1605.

[14] J.P. Holman, *Heat Transfer*, McGraw-Hill 10th Ed. (2010).

[15] ANSYS, Academic Research, Release 18.0.

[16] R.F. Warming, R.M. Beam, Upwind second-order difference schemes and applications in aerodynamic flows, *AIAA Journal*, 14 (1976) 1241-1249.

[17] OXYCHEM, *Caustic Potash Handbook*, Occidental Chemical Corporation (2013) 39.

[18] C. Habchi and T. Lemenand and D. D. Valle and H. Peerhossaini, Turbulence behavior of artificially generated vorticity, *Journal of Turbulence*, 11 (2010) N36.

[19] I. Celik, U. Ghia, P. Roache, H. Freitas, Procedure for estimation and reporting of uncertainty due to discretization in CFD applications, *Journal of Fluids Engineering*, 130 (2008) 078001.